Applied Physics Letters

RESEARCH ARTICLE | APRIL 30 2024

Magnon spin capacitor

Special Collection: Magnonics

Pieter M. Gunnink ; Tim Ludwig ; Rembert A. Duine

Check for updates

Appl. Phys. Lett. 124, 182404 (2024)
https://doi.org/10.1063/5.0201442

View Online
Export Citation

05 June 2024 12:30:36

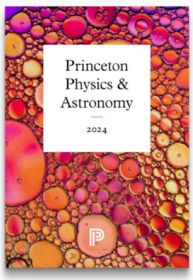

Browse our new Physics and Astronomy Catalog
30% off titles with code **P326**

PRINCETON UNIVERSITY PRESS

AIP Publishing

Applied Physics Letters ARTICLE pubs.aip.org/aip/apl

Magnon spin capacitor

Cite as: Appl. Phys. Lett. **124**, 182404 (2024); doi: 10.1063/5.0201442
Submitted: 30 January 2024 · Accepted: 18 April 2024 ·
Published Online: 30 April 2024

View Online Export Citation CrossMark

Pieter M. Gunnink,[1,a)] Tim Ludwig,[1] and Rembert A. Duine[1,2]

AFFILIATIONS

[1]Institute for Theoretical Physics and Center for Extreme Matter and Emergent Phenomena, Utrecht University, Princetonplein 5, 3584 CC Utrecht, The Netherlands
[2]Department of Applied Physics, Eindhoven University of Technology, P.O. Box 513, 5600 MB, Eindhoven, The Netherlands

Note: This paper is part of the APL Special Collection on Magnonics.
[a)]**Present address:** Institute of Physics, Johannes Gutenberg-University Mainz, Staudingerweg 7, Mainz 55128, Germany.
Author to whom correspondence should be addressed: pgunnink@uni-mainz.de

ABSTRACT

In this work, we show that a magnon spin capacitor can be realized at a junction between two exchange coupled ferromagnets. In this junction, the buildup of magnon spin over the junction is coupled to the difference in magnon chemical potential, realizing the magnon spin analogue of an electrical capacitor. The relation between magnon spin and magnon chemical potential difference directly follows from considering the magnon density–density interaction between the two ferromagnets. We analyze the junction in detail by considering spin injection and detection from normal metal leads, the tunneling current across the junction, and magnon decay within the ferromagnet, showing that such a structure realizes a magnon spin capacitor in series with a spin resistor. Choosing yttrium iron garnet as the ferromagnet, we numerically calculate the magnon spin capacitance which ranges from picofarad to microfarad, depending on the area of the junction. We therefore conclude that the magnon spin capacitor could directly be of use in applications.

Published under an exclusive license by AIP Publishing. https://doi.org/10.1063/5.0201442

05 June 2024 12:30:36

Spintronics aims to replace charge with the spin degree of freedom, in particular targeting the replacement of conventional CMOS technology. A number of spintronics circuit elements have to date been implemented, such as spin transistors[1] and methods for efficient spin transport.[2,3] Less attention has been paid to designing a spin capacitor, a spintronic analogue of the electrical capacitor. Analogous to electrical capacitors,[4] spin capacitors are important for the fast manipulation of spin systems, because of their frequency-dependent response. Previously, proposals for a spin capacitor have either employed conventional electrical capacitors combined with spin polarization[5–7] or magnetic tunneling junctions,[8–11] having to deal with short spin decoherence times, or were only concerned with the storage of spin over long timescales,[12] neglecting the important frequency response.

In this work, we theoretically propose how to realize a magnon spin capacitor, employing magnons, or spin waves, as spin carriers.[13,14] Because magnons have fast-response times and are long lived, the magnon spin capacitor functions over a wide frequency range, proving its usefulness in spintronics.

We consider a ferromagnetic junction with a general XXZ type coupling as shown in Fig. 1(a) and obtain the fundamental magnon spin capacitor relation,

$$dQ_m = C_m dV_m, \tag{1}$$

where $Q_m \equiv \hbar(n_L - n_R)$ is the relative magnon spin, defined as the buildup in the magnon number $n_{L/R}$ over the junction, and $V_m \equiv \mu_m^L - \mu_m^R$ is the magnon spin accumulation bias, defined as the difference in magnon chemical potentials $\mu_m^{L/R}$. Left (L) and right (R) indicate the left and right ferromagnet. Finally, C_m is a coefficient relating the two quantities, which we identify as the magnon spin capacitance. Importantly, this is the direct result of considering the density–density interaction, coupling the S^z components of the spins in the left and right ferromagnet—in analogy with the Coulomb interaction in the electrical capacitor.

Our proposal realizes a magnon spin capacitor in a ferromagnetic junction similar to those used in magnon spin valve experiments.[15] We consider both a parallel and antiparallel configuration of the magnetization and show that the magnon capacitance can be tuned by the alignment. To connect to a possible experimental setup, we include the injection and detection of spin through normal metal leads—creating the magnonic circuit as shown in Fig. 1(b). Finally, we show that the quantum magnon capacitance plays a role at low temperatures and discuss how it is related to the instability of the antiparallel configuration of the magnetization.

We consider a junction of two ferromagnetic insulators, as depicted in Fig. 1(a). The dynamics of the spins $\boldsymbol{S}_i$ with length S in the bulk of each ferromagnet are modeled by the Hamiltonian,

Published under an exclusive license by AIP Publishing

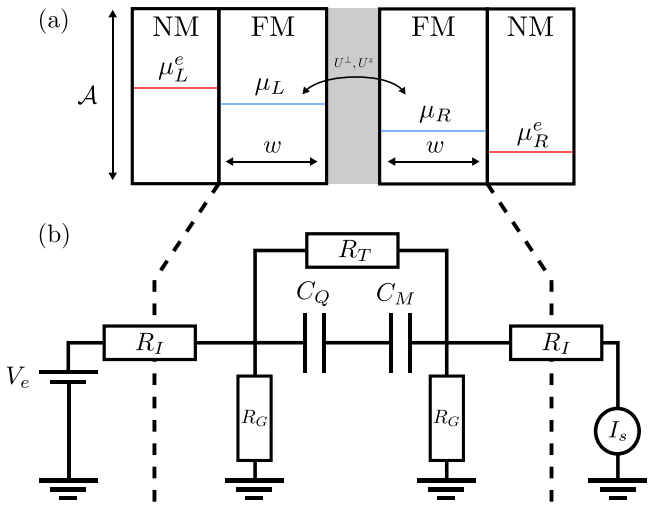

FIG. 1. (a) The ferromagnetic (FM) junction with attached normal metal (NM) leads considered in this work. (b) The circuit representation of the junction. A spin bias is applied through the spin accumulation $\mu^e_{L/R}$ in the left/right normal metal lead, driving the magnon chemical potentials $\mu_m^{L/R}$. The left and right ferromagnet with width w and surface area $\mathcal{A}$ are coupled through an XXZ coupling with strengths $U^\perp$ and U^z, giving rise to a tunneling current (represented by the resistance R_T) and a magnon capacitance, represented by two capacitors in series, related to the quantum magnon capacitance C_Q and to the mutual interaction C_M. The resistors R_I represent the interfacial resistance of the NM|FM interface and the resistors R_G the magnon decay. The spin current injected in the right normal metal lead, I_s, can be measured through the inverse spin Hall effect.

$$\mathcal{H}_{L/R} = -\frac{1}{2}\sum_{ij} J_{L/R,ij}\boldsymbol{S}_{L/R,i}\cdot\boldsymbol{S}_{L/R,j} - h_{L/R}\sum_i S^z_{L/R,i}, \tag{2}$$

where i and j label the lattice sites, $J_{L/R,ij}$ is the exchange coupling, which we take to be nearest neighbor with strength $J_{L/R,ij} \equiv J_{L/R} > 0$ and $h_{L/R} \equiv \hbar\gamma_{L/R}\mu_0 H_{L/R}$ is the Zeeman energy, with $\gamma_{L/R}$ the gyromagnetic ratio and $\mu_0 H_{L/R}$ the magnetic field in the left or right ferromagnet, which can be positive or negative, allowing for a parallel or antiparallel alignment of the spins with the z-axis.

We apply the Holstein–Primakoff transformation, $S^-_{L/R,i} \simeq \sqrt{2S}b_{L/R,i} + O(S^{-1/2})$ and $S^{z,\uparrow}_{L/R,i} = S - b^\dagger_{L/R,i}b_{L/R,i}$ or $S^{z,\downarrow}_{L/R,i} = -S + b^\dagger_{L/R,i}b_{L/R,i}$.[16] Here, $\uparrow$ and $\downarrow$ refer to the parallel and antiparallel alignment of the spins with the z-axis. The spin Hamiltonian (2) is then diagonalized through the Fourier transformation $b_{L/R,i} = 1/\sqrt{N_{L/R}}\sum_{\boldsymbol{k}} e^{i\boldsymbol{k}\cdot\boldsymbol{r}_i} b_{L/R,\boldsymbol{k}}$ to obtain $\mathcal{H}_{L/R} = \sum_{\boldsymbol{k}} \hbar\omega_{L/R,\boldsymbol{k}} b^\dagger_{L/R,\boldsymbol{k}} b_{L/R,\boldsymbol{k}}$. In what follows, we work in the long-wavelength limit, such that $\hbar\omega_{L/R,\boldsymbol{k}} = \Delta_{L/R} + J_{L/R,s}k^2$, where $\Delta_{L/R} \equiv \hbar\gamma_{L/R}\mu_0 H_{L/R}$ is the magnon gap and $J_{L/R,s} \equiv J_{L/R}S_{L/R}a^2_{L/R}$ is the spin stiffness, with $a_{L/R}$ the lattice constant. The coupling between two isotropic ferromagnetic insulators can typically be described as an effective XXZ type coupling, $\mathcal{H}_c = \mathcal{H}_\perp + \mathcal{H}_z$, where $\mathcal{H}_\perp = -\sum_{ij} U^\perp_{ij}(S^x_{L,i}S^x_{R,j} + S^y_{L,i}S^y_{R,j})$ and $\mathcal{H}_z = -\sum_{ij} U^z_{ij}S^z_{L,i}S^z_{R,j}$, with $U^\perp_{ij}$ and U^z_{ij} the transverse and longitudinal exchange coupling, respectively. For the relative parallel (P) and antiparallel (AP) configurations of the magnetization, we obtain, after applying the Holstein–Primakoff transformation,

$$\mathcal{H}^P_\perp = -\sqrt{\frac{S_L S_R}{N_L N_R}}\sum_{\boldsymbol{k}\boldsymbol{k}'} U^\perp_{\boldsymbol{k}\boldsymbol{k}'}(b_{L,\boldsymbol{k}}b^\dagger_{R,\boldsymbol{k}'} + \text{H.c.}), \tag{3}$$

$$\mathcal{H}^P_z = -U^z_0\sum_{\boldsymbol{k}\boldsymbol{k}'} n_{L,\boldsymbol{k}}n_{R,\boldsymbol{k}'}, \tag{4}$$

$$\mathcal{H}^{AP}_\perp = -\sqrt{\frac{S_L S_R}{N_L N_R}}\sum_{\boldsymbol{k}\boldsymbol{k}'} U^\perp_{\boldsymbol{k}\boldsymbol{k}'}(b^\dagger_{L,\boldsymbol{k}}b^\dagger_{R,\boldsymbol{k}'} + b_{L,\boldsymbol{k}}b_{R,\boldsymbol{k}'}), \tag{5}$$

$$\mathcal{H}^{AP}_z = +U^z_0\sum_{\boldsymbol{k}\boldsymbol{k}'} n_{L,\boldsymbol{k}}n_{R,\boldsymbol{k}'}, \tag{6}$$

where $n_{L/R,\boldsymbol{k}} \equiv b^\dagger_{L/R,\boldsymbol{k}}b_{L/R,\boldsymbol{k}}$ is the magnon number operator, $U^\perp_{\boldsymbol{k}\boldsymbol{k}'} \equiv \sum_{ij} e^{-i\boldsymbol{k}\cdot\boldsymbol{r}_i}e^{-i\boldsymbol{k}'\cdot\boldsymbol{r}_j}U^\perp_{ij}$ is the scattering rate, and $U^z_0 \equiv \sum_{ij}\frac{U^z_{ij}}{N_L N_R}$ is the density–density interaction strength. We have performed the usual expansion in large S, but have kept the magnon density-density interaction, $\propto n_{L,\boldsymbol{k}}n_{R,\boldsymbol{k}'}$, that couples the magnon densities of the two subsystems. We disregard constant energy shifts, which do not play a role in the dynamics. The density–density interaction strength U^z_0 is directly related to the classical energy of the system and can thus be experimentally determined, which we discuss in more detail in the supplementary material. Finally, we note that in the antiparallel configuration there is no tunneling allowed between the left and right subsystem, since the magnon excitations are orthogonal to each other.

Central to our work is the magnon density–density interaction, described by Eqs. (4) and (6). This interaction is quartic in magnon operators and can therefore not be brought to a diagonalized form. However, if the coupling energy scale, set by U^z_0, is small compared to the bulk energy scales, we can employ a mean-field approach. The left/right magnon distribution function is then

$$n_{L/R,\boldsymbol{k}} = f_B\left(\frac{\hbar\omega_{L/R,\boldsymbol{k}} + U_{L/R} - \mu_m^{L/R}}{k_B T_{L/R}}\right), \tag{7}$$

where $f_B(x) = 1/(e^x - 1)$ is the Bose function and $U_{L/R} \equiv \mp U^z_0 \times \sum_{\boldsymbol{k}'} n_{R/L,\boldsymbol{k}'}$ is the energy as a result of the density–density interaction with the second ferromagnet, thus coupling the magnon distribution of the left ferromagnet with the right ferromagnet as a shift of the right magnon band and vice versa. Here, $\mp$ indicates the parallel (–) and antiparallel (+) configuration. We have introduced the magnon chemical potential $\mu_m^{L/R}$ for the left/right ferromagnet to parametrize a long-living nonequilibrium magnon state, which is justified on time scales longer than the number-conserving exchange driven magnon–magnon scattering time.[3]

For simplicity, we assume the left and right ferromagnets to be identical, i.e., $\omega_{L,\boldsymbol{k}} = \omega_{R,\boldsymbol{k}} \equiv \omega_{\boldsymbol{k}}$ and consider equal temperatures, $T_L = T_R \equiv T$. To determine the non-equilibrium response, we expand the magnon distribution as $n_{L/R,\boldsymbol{k}} = n^0_{\boldsymbol{k}} + \delta n_{L/R,\boldsymbol{k}}$, where $n^0_{\boldsymbol{k}}$ is the equilibrium magnon distribution and $\delta n_{L/R,\boldsymbol{k}}$ the non-equilibrium response. The potential energy is now written as an effective energy shift, $U_{L/R} = \mp U^z_0\sum_{\boldsymbol{k}'} n^0_{\boldsymbol{k}'} + \delta n_{R/L,\boldsymbol{k}'}$. Assuming that both $\mu_m^{L/R} \ll \Delta$ and $U_{L/R} \ll \Delta$, we expand the magnon distribution function, Eq. (7), in $\mu_m^{L/R}$ and $U_{L/R}$ to find

$$\delta n_{L,\boldsymbol{k}} = -\frac{\partial n^0_{\boldsymbol{k}}}{\partial\omega_{\boldsymbol{k}}}\left[\mu_m^L \mp U^z_0\sum_{\boldsymbol{k}'}(n^0_{\boldsymbol{k}'} + \delta n_{R,\boldsymbol{k}'})\right], \tag{8}$$

05 June 2024 12:30:36

Published under an exclusive license by AIP Publishing

$$\delta n_{R,\boldsymbol{k}} = -\frac{\partial n^0_{\boldsymbol{k}}}{\partial \omega_{\boldsymbol{k}}}\left[\mu^R_m \pm U^z_0 \sum_{\boldsymbol{k}'}\left(n^0_{\boldsymbol{k}'} + \delta n_{L,\boldsymbol{k}'}\right)\right], \tag{9}$$

where we used $n^0_{\boldsymbol{k}} = f_B(\hbar\omega_{\boldsymbol{k}}/k_BT)$. These coupled equations describe the response of the system to a change in the magnon number through one of two ways: (1) changing the chemical potential and (2) shifting the bottom of the band.[17] The bottom of the band is set by the mutual density–density interaction, thus coupling the two equations. Equations (8) and (9) are now solved for $\delta n_{L/R,\boldsymbol{k}}$ to find the relative magnon spin,

$$Q_m = -\hbar \sum_{\boldsymbol{k}} \frac{\partial n^0_{\boldsymbol{k}}}{\partial \hbar\omega_{\boldsymbol{k}}}\left(V_m \mp U^z_0 Q_m/\hbar\right), \tag{10}$$

where $Q_m \equiv \hbar\sum_{\boldsymbol{k}}(n_{L,\boldsymbol{k}} - n_{R,\boldsymbol{k}})$ and $V_m \equiv \mu^L_m - \mu^R_m$. Now, we solve Eq. (10) to obtain Q_m and take the derivative with respect to V_m to obtain the central result of this work: the fundamental magnon spin capacitor equation (1). Explicitly, we find the capacitance as

$$\frac{1}{C_m} = \frac{1}{C_Q} \pm \frac{1}{C_M}, \tag{11}$$

where

$$C_Q = -\hbar\mathcal{V}\int \frac{d^3k}{(2\pi)^3}\frac{\partial f_B\left(\frac{\hbar\omega_{\boldsymbol{k}}}{k_BT}\right)}{\partial \hbar\omega_{\boldsymbol{k}}} \tag{12}$$

is the quantum magnon capacitance (converted to an integral in the thermodynamic limit) and

$$C_M = \frac{\hbar}{\mathcal{U}^z}\mathcal{A} \tag{13}$$

is the mutual magnon capacitance. Here, we used the fact that, for sufficiently large systems, the interaction U^z_{ij} is local and translationally invariant, such that we can write $U^z_0 = \mathcal{U}^z/\mathcal{A}$, where $\mathcal{A}$ is the interfacial surface area of the ferromagnet and $\mathcal{U}^z$ is the interfacial coupling energy. We refer the reader to the supplementary material for more details regarding the area scaling.

The Hamiltonian $\mathcal{H}_\perp$ yields a tunneling current $I_s = \sigma_T(\mu^L_m - \mu^R_m)$, between the two magnon subsystems, if $U^\perp_{\boldsymbol{k}\boldsymbol{k}'}$ is small compared to the bulk energy scales.[18] We give σ_T in the supplementary material. Note that in the antiparallel configuration $\sigma_T = 0$ [cf. Eq. (5)].

From Eq. (1), we obtain the relation of the magnon current through the system, $I_m \equiv \dot{Q}_m$, in response to the rate of change in magnon spin accumulation, $\dot{V}_m$, as $I_m(t) = C_m\dot{V}_m(t)$. In the parallel configuration, there will be a leakage current flowing between the left and right ferromagnet, acting as an additional resistor in parallel to the capacitor with resistance $R^{-1}_T \equiv \sigma_T$. We therefore represent the magnonic capacitor with the circuit representation in Fig. 1(b), consisting of a mutual and quantum capacitor in series, parallel to a resistor.

The magnon capacitor offers an additional engineering degree of freedom: the choice between a parallel and antiparallel configuration, which switches the sign of the mutual magnon capacitance C_M and changes the leakage current I_s from finite to zero. The switching of the sign of the mutual magnon capacitance is the effect of the interfacial exchange coupling, which energetically prefers a parallel alignment for $U^z_0 > 0$. The buildup of relative magnon spin Q_m thus increases the total energy of the system in the parallel alignment, whereas in the antiparallel alignment, the total energy is decreased. Increasing the magnon number also incurs an energetic cost due to the Bose–Einstein statistics, described by the quantum magnon capacitance. In the antiparallel configuration, there thus exists an energetic instability if $C^{AP}_M > C_Q$, beyond which the linear spin-wave theory employed here is no longer valid.

We next consider the magnon capacitor in a structure with normal metal leads attached, demonstrating a simple magnonic circuit that can be realized with the magnon capacitor. An attached normal metal (NM) lead to a ferromagnet (FM) will drive a spin current across the NM|FM interface given by $I_{L/R} = \sigma_I(\mu^e_{L/R} - \mu^{L/R}_m)$, where σ_I is given in the supplementary material. The resistance of the NM|FM interface is then $R^{-1}_I \equiv \sigma_I$.

The magnon number is not a conserved quantity, and magnons will decay through several processes, such as magnon–phonon scattering. This effect can be modeled with a resistor to ground, with a resistance $R^{-1}_G = \mathcal{V}\sigma_G$, where σ_G is the spin-relaxation conductance, which we obtain from experimental measurements.

The total work done will be $dW_m = V_m dQ_m/\hbar$, such that the total energy stored in the magnon capacitor is

$$E = \frac{1}{\hbar}\frac{Q^2_m}{2C_m} = \frac{1}{2}\frac{C_m}{\hbar}V^2_m. \tag{14}$$

From this expression for the energy, it is clear that the energy is stored in the buildup of relative magnon spin Q_m over the capacitor, mediated by the mutual interaction, i.e., the energy due to the interactions between magnons in the left and right ferromagnet that results from the density–density interaction. Since magnons have a finite lifetime, this is not a perfect magnon spin battery and will drain over a timescale set by R_GC_m.

Attaching normal metal leads to the ferromagnetic junction corresponds to the magnonic circuit as shown in Fig. 1, where a spin-accumulation bias $V_e = \mu^e_L - \mu^e_R$ is applied to the magnon capacitor, consisting of two capacitors in series, representing the quantum magnon capacitance C_Q and mutual interaction C_M, with a parallel leakage resistor. The finite magnon lifetime is parametrized with two resistors to ground. This circuit can then be analyzed using conventional circuit analysis. As we will show later, for typical parameters, the magnon decay resistance R_G and tunneling resistance R_T are large, while the resistance of the NM|FM interface is small, and they can thus be effectively disregarded. The circuit can therefore be treated as a capacitor, where the injected spin current in the right normal metal, $I_s(t)$ in Fig. 1(b), can be measured (through the inverse spin Hall effect). In addition, this capacitor can of course be embedded in a larger spintronics circuit, disregarding the need for electrical injection and detection of spin altogether.

In this work, we propose the simplest RC-circuit, which can be built with the magnon spin capacitor, where an additional resistor with resistance R is placed in series with the spin capacitor to realize an RC-circuit. We then obtain for the DC response, with the capacitor initially uncharged and at $t = 0$ an external spin bias is applied, $I_s(t) = \frac{V_e}{R}e^{-t/\tau}$, where $\tau \equiv RC$ is the time constant of this system, also known as the RC time. Since the magnon capacitance can switch sign between the parallel and antiparallel configuration, τ can have either sign and thus, the magnon current can increase exponentially—reversing the magnetization, unless it is limited by non-linear

05 June 2024 12:30:36

Published under an exclusive license by AIP Publishing

interactions. The AC response is a high-pass filter, $I_s(\omega) = \frac{1}{R}\frac{i\tau\omega}{1+i\tau\omega}V_e(\omega)$, with cutoff frequency $\omega_c \equiv \tau^{-1}$ and associated frequency-dependent phase shift $\tan\phi \equiv (\omega\tau)^{-1}$.

We now numerically calculate the capacitance and resistances, considering both ferromagnetic insulators to be yttrium iron garnet (YIG), such that $S = 14.2$, $J_s = 8.5 \times 10^{-40}\mathrm{Jm}^2$ and we take $\Delta/k_B = 1\mathrm{K}$.[19] Furthermore, we assume a rough interface with an isotropic exchange coupling, such that scattering of the incident magnons does not conserve momentum and we have a tunneling amplitude $U^{\perp}_{\boldsymbol{k}\boldsymbol{k}'} \approx U^{\perp}$. The normal metals we assume to be platinum (Pt), with the spin-mixing conductance for the Pt|YIG interface given by $g^{\uparrow\downarrow} = 1.6 \times 10^{14}\,\mathrm{S/m}^2$.[20,21] In what follows, we quote capacitances and resistances in electrical units, by assigning magnons a charge e and expressing the chemical potential V in voltage, i.e., $Q_m \to Q_m\, e/\hbar$ and $V_m \to V_m/e$, such that $C \to C\, e^2/\hbar$ and $R \to R\,\hbar/e^2$.

Motivated by recent magnon valve experiments,[15,22] we assume a coupling strength $\mathcal{U}^z/a^2$ and tunneling amplitude $U^{\perp}$ of 1–100 μeV. This interfacial coupling can originate from the Ruderman–Kittel–Kasuya–Yosida (RKKY) coupling,[23–25] or from magnetostatic coupling through the dipole–dipole interaction.[26,27]

For a device of $1 \times 1 \times 1\,\mu$m and $\mathcal{U}^z/a^2 = U^{\perp} = 10\,\mu$eV at room temperature, we find $C_M \approx 10\,$nF and $C_Q \approx 50\,$nF. Therefore, neither capacitance can be disregarded and remains relevant, in contrast to the electronic case, where the quantum capacitance can usually be neglected for macroscopic devices. The Pt|YIG interfacial resistance is $R_I \approx 0.3\,\Omega$, and the tunneling resistance (in the parallel orientation) between the two ferromagnets is $R_T \approx 600\,\mathrm{M}\Omega$. Furthermore, for YIG at room temperature $\sigma_G = 5\,\mathrm{mS}/\mu\mathrm{m}^3$ and thus $R_G \approx 200\,\Omega$.[3]

The magnon chemical potential and thus the magnon capacitance are only well defined on timescales slower than the magnon–magnon scattering timescale, which is approximately 10^{-13} s in YIG at room temperature.[3,28] The magnon spin capacitor will additionally discharge over a timescale set by $C_m R_G$, which is 10^{-6} s for the same parameters. Therefore, the magnon spin capacitor functions over a wide timescale. In addition, the magnon spin diffusion length, which is 10 μm in YIG at room temperature,[3] sets the length scale over which the chemical potential can be regarded as constant, beyond which additional modifications of our theory are necessary.

We show the total capacitance in Fig. 2 as a function of the surface area $\mathcal{A}$. Here, the dashed line indicates the quantum capacitance C_Q, which serves as an upper limit [cf. Eq. (11)]. We observe that the capacitance can be tuned over a wide range through the surface area, similar to how surface area in electronics is used to obtain the desired electrical capacitance.

We now consider the effect of temperature on the capacitance in Fig. 3, where we show the ratio C_M/C_Q together with the total capacitance C_m in the parallel and antiparallel configuration. For low temperatures, $C_Q < C_M$ and thus $C_m \approx C_Q$. At higher temperatures, the quantum capacitance reduces and the mutual magnon capacitance becomes relevant, and $C_m \approx C_M$ in the high-temperature limit.

In the antiparallel orientation, the quantum and mutual magnon capacitance compete [as can be seen from the minus sign in Eq. (11)], and thus, the total capacitance diverges, which will result in a divergence of the RC time—beyond which the antiparallel orientation is unstable. This is due to the fact that the thermal magnons now have sufficient energy to overcome the mutual interaction energy. The divergence is thus related to a bosonic Stoner-like instability, i.e., the

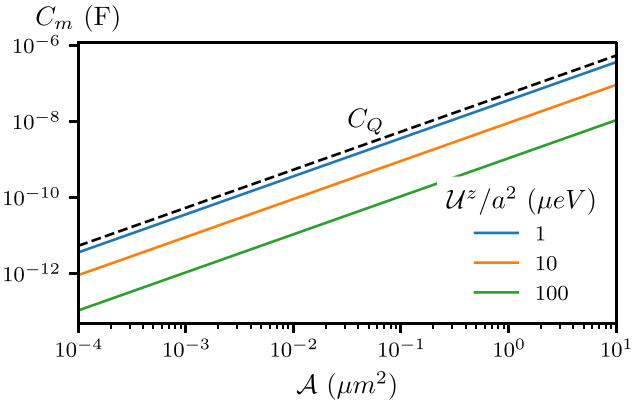

FIG. 2. The total capacitance C_m in the parallel orientation at room temperature $T = 290\mathrm{K}$, as a function of the surface area $\mathcal{A}$, for varying interaction strength $\mathcal{U}^z$. The dashed line indicates C_Q, which provides as an upper limit for the total capacitance [cf. Eq. (11)].

trade-off between kinetic and interaction energies.[29,30] We note that for our choice of parameters and materials this divergence occurs at approximately 60 K, but this is strongly dependent on both the dimensions of the device and the coupling strength.

In conclusion, we have shown that a ferromagnetic junction functions as a magnon spin capacitor, thus providing a key element for spintronic circuits. We have derived the fundamental capacitor equation (1) coupling the relative magnon spin Q_m to the magnon spin accumulation bias V_m through a magnon spin capacitance C_m, with contributions from the mutual magnon capacitance and the quantum magnon capacitance. When normal metal leads and an additional resistor are attached, this device can be readily used in an RC circuit. Finally, we showed that a wide parameter range is available. We therefore also conclude that the magnon spin capacitor as considered in this work could be directly of use in applications.

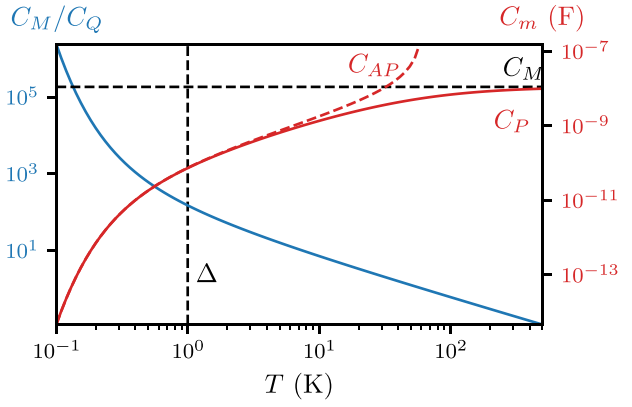

FIG. 3. The ratio between the mutual and quantum magnon capacitance (blue solid, left axis) and the total capacitance C_m in the parallel orientation (red solid, right axis) and antiparallel orientation (red dashed, right axis), as a function of temperature. Here, $\mathcal{U}^z/a^2 = 10\,\mu$eV and device size is $1 \times 1 \times 1\,\mu\mathrm{m}^3$. The horizontal dashed line indicates C_M, which is independent of temperature and the vertical dashed line indicates the magnon gap $\Delta = 1\,\mathrm{K}$.

05 June 2024 12:30:36

Published under an exclusive license by AIP Publishing

See the supplementary material for more details on the density–density interaction and expressions for σ_T and σ_I, which includes Refs. 31–35.

R.A.D. is a member of the D-ITP consortium, a program of the Dutch Research Council (NWO), funded by the Dutch Ministry of Education, Culture and Science (OCW). This work is a part of the research programme Fluid Spintronics with Project No. 182.069, financed by the Dutch Research Council (NWO).

AUTHOR DECLARATIONS

Conflict of Interest

The authors have no conflicts to disclose.

Author Contributions

Pieter M. Gunnink: Conceptualization (supporting); Investigation (lead); Methodology (lead); Writing – original draft (lead); Writing – review & editing (lead). **Tim Ludwig:** Conceptualization (supporting); Investigation (supporting); Methodology (supporting); Writing – review & editing (supporting). **Rembert A. Duine:** Conceptualization (lead); Investigation (supporting); Methodology (supporting); Writing – review & editing (supporting).

DATA AVAILABILITY

Data sharing is not applicable to this article as no new data were created or analyzed in this study.

REFERENCES

[1]S. Datta and B. Das, "Electronic analog of the electro-optic modulator," Appl. Phys. Lett. **56**, 665–667 (1990).
[2]*Handbook of Spin Transport and Magnetism*, edited by E. Y. T. ZuticIgor (Chapman and Hall/CRC, New York, 2012).
[3]L. J. Cornelissen, K. J. H. Peters, G. E. W. Bauer, R. A. Duine, and B. J. van Wees, "Magnon spin transport driven by the magnon chemical potential in a magnetic insulator," Phys. Rev. B **94**, 014412 (2016).
[4]P. Horowitz and W. Hill, *The Art of Electronics*, 3rd ed. (Cambridge University Press, New York, 2015).
[5]A. Brataas, Y. V. Nazarov, J. Inoue, and G. E. W. Bauer, "Spin accumulation in small ferromagnetic double-barrier junctions," Phys. Rev. B **59**, 93–96 (1999).
[6]S. Datta, "Proposal for a "spin capacitor,"" Appl. Phys. Lett. **87**, 013115 (2005).
[7]Y. G. Semenov, J. M. Zavada, and K. W. Kim, "Graphene spin capacitor for magnetic field sensing," Appl. Phys. Lett. **97**, 013106 (2010).
[8]G. Landry, Y. Dong, J. Du, X. Xiang, and J. Q. Xiao, "Interfacial capacitance effects in magnetic tunneling junctions," Appl. Phys. Lett. **78**, 501–503 (2001).
[9]S. T. Chui and L. Hu, "Ac transport in ferromagnetic tunnel junctions," Appl. Phys. Lett. **80**, 273–275 (2002).
[10]H. Kaiju, S. Fujita, T. Morozumi, and K. Shiiki, "Magnetocapacitance effect of spin tunneling junctions," J. Appl. Phys. **91**, 7430–7432 (2002).
[11]Y.-H. Zhu, X.-X. Zhang, J. Liu, and P.-S. He, "Spin-accumulation capacitance and its application to magnetoimpedance," J. Appl. Phys. **122**, 043902 (2017).
[12]T. Moorsom, M. Rogers, I. Scivetti, S. Bandaru, G. Teobaldi, M. Valvidares, M. Flokstra, S. Lee, R. Stewart, T. Prokscha, P. Gargiani, N. Alosaimi, G. Stefanou, M. Ali, F. Al Ma'Mari, G. Burnell, B. J. Hickey, and O. Cespedes, "Reversible spin storage in metal oxide-fullerene heterojunctions," Sci. Adv. **6**, eaax1085 (2020).
[13]V. V. Kruglyak, S. O. Demokritov, and D. Grundler, "Magnonics," J. Phys. D: Appl. Phys. **43**, 264001 (2010).
[14]A. V. Chumak, P. Kabos, M. Wu, C. Abert, C. Adelmann, A. O. Adeyeye, J. Åkerman, F. G. Aliev, A. Anane, A. Awad, C. H. Back, A. Barman, G. E. W. Bauer, and X. Zhang, "Advances in magnetics roadmap on spin-wave computing," IEEE Trans. Magn. **58**, 1–72 (2022).
[15]H. Wu, L. Huang, C. Fang, B. S. Yang, C. H. Wan, G. Q. Yu, J. F. Feng, H. X. Wei, and X. F. Han, "Magnon valve effect between two magnetic insulators," Phys. Rev. Lett. **120**, 097205 (2018).
[16]T. Holstein and H. Primakoff, "Field dependence of the intrinsic domain magnetization of a ferromagnet," Phys. Rev. **58**, 1098–1113 (1940).
[17]M. Büttiker, H. Thomas, and A. Prêtre, "Mesoscopic capacitors," Phys. Lett. A **180**, 364–369 (1993).
[18]J. Zheng, A. Rückriegel, S. A. Bender, and R. A. Duine, "Ellipticity and dissipation effects in magnon spin valves," Phys. Rev. B **101**, 094402 (2020).
[19]V. Cherepanov, I. Kolokolov, and V. L'vov, "The saga of YIG: Spectra, thermodynamics, interaction and relaxation of magnons in a complex magnet," Phys. Rep. **229**, 81–144 (1993).
[20]J. Flipse, F. K. Dejene, D. Wagenaar, G. E. W. Bauer, J. B. Youssef, and B. J. van Wees, "Observation of the spin Peltier effect for magnetic insulators," Phys. Rev. Lett. **113**, 027601 (2014).
[21]J. Xiao and G. E. W. Bauer, "Transport between metals and magnetic insulators," arXiv:1508.02486 [cond-mat] (2015).
[22]Q. Chen, X. Ruan, H. Yuan, X. Zhou, Z. Kou, Z. Huang, Y. Xu, and Y. Zhai, "Interlayer transmission of magnons in dynamic spin valve structures," Appl. Phys. Lett. **116**, 132403 (2020).
[23]M. A. Ruderman and C. Kittel, "Indirect exchange coupling of nuclear magnetic moments by conduction electrons," Phys. Rev. **96**, 99–102 (1954).
[24]T. Kasuya, "A theory of metallic ferro- and antiferromagnetism on Zener's model," Prog. Theor. Phys. **16**, 45–57 (1956).
[25]K. Yosida, "Magnetic properties of Cu-Mn alloys," Phys. Rev. **106**, 893–898 (1957).
[26]S. O. Demokritov, A. A. Serga, A. André, V. E. Demidov, M. P. Kostylev, B. Hillebrands, and A. N. Slavin, "Tunneling of dipolar spin waves through a region of inhomogeneous magnetic field," Phys. Rev. Lett. **93**, 047201 (2004).
[27]T. Schneider, A. A. Serga, A. V. Chumak, B. Hillebrands, R. L. Stamps, and M. P. Kostylev, "Spin-wave tunnelling through a mechanical gap," Europhys. Lett. **90**, 27003 (2010).
[28]S. A. Bender, R. A. Duine, A. Brataas, and Y. Tserkovnyak, "Dynamic phase diagram of dc-pumped magnon condensates," Phys. Rev. B **90**, 094409 (2014).
[29]J. Armaitis and R. A. Duine, "Superfluidity and spin superfluidity in spinor Bose gases," Phys. Rev. A **95**, 053607 (2017).
[30]J. Radić, S. S. Natu, and V. Galitski, "Stoner ferromagnetism in a thermal pseudospin-1/2 Bose gas," Phys. Rev. Lett. **113**, 185302 (2014).
[31]J. Hick, F. Sauli, A. Kreisel, and P. Kopietz, "Bose-Einstein condensation at finite momentum and magnon condensation in thin film ferromagnets," Eur. Phys. J. B **78**, 429–437 (2010).
[32]T. Cookmeyer and S. D. Sarma, "Symmetry breaking in zero field 2D electron bilayers," arXiv:2312.10791 (2023).
[33]S. A. Bender, R. A. Duine, and Y. Tserkovnyak, "Electronic pumping of quasiequilibrium Bose-Einstein-condensed magnons," Phys. Rev. Lett. **108**, 246601 (2012).
[34]S. A. Bender and Y. Tserkovnyak, "Interfacial spin and heat transfer between metals and magnetic insulators," Phys. Rev. B **91**, 140402(R) (2015).
[35]R. A. Duine, A. Brataas, S. A. Bender, and Y. Tserkovnyak, "Spintronics and magnon Bose-Einstein condensation," in *Universal Themes of Bose-Einstein Condensation*, edited by D. W. Snoke, N. P. Proukakis, and P. B. Littlewood (Cambridge University Press, Cambridge, 2017), pp. 505–524.

05 June 2024 12:30:36

Published under an exclusive license by AIP Publishing